Monte-Carlo simulation of Baroclinic Vortices in the Heton Model

By
Syed M. Assad, Physics Department, National University of Singapore, Singapore
and
Chjan C. Lim, Mathematical Sciences, Rensselaer Polytechnic Institute
Troy, NY 12180, USA
+

Abstract

This paper examines the practicality of using a Monte Carlo algorithm to analyze the point-vortex equilibrium statistical model of two layers baroclinic quasigeostrophic vortices in the two dimensional plane. The conserved quantity, angular momentum, serves to confine the vortices, eliminating the need for complicated boundary conditions. This method provides a fast and efficient algorithm for solving the mean field nonlinear elliptic PDEs of the equilibrium statistical theory. A verification of the method is done by comparison with the exact Gaussian solution at inverse temperature zero. The numerical results obtained include a geophysically and computationally relevant power law for the radii of the supports of the most probable vorticity distributions: For fixed total circulations, and fixed average angular momentum, the radii of both layers are proportional to the square-root of the inverse temperature β. This confirms that the most probable vorticities are supported on disks of finite radii. By changing the chemical potentials μ of the runs, one is able to model the most probable vorticity distributions for a wide range of total circulations and energy on a fixed disk (of fixed radius) with zero boundary conditions on the bounding circle. The radially symmetric most probable vorticities at positive temperatures are consistently, near flat-top profiles for the layer with the greater total circulation, and near Gaussian profiles for the layer with the weaker circulation.

Keywords: Heton model, statistical mechanics, Monte Carlo simulation, mean field theory.

1 Introduction

The Monte Carlo algorithm had been previously used in the study of equilibrium statistical mechanics of vortices in fluid dynamics. In this paper, we extend its use to an unbounded two layer baroclinic point vortex model.

In this model developed by DiBattista and Madja [1], the rotational invariance of the Hamiltonian and domain give rise to an angular momentum constrain. In the same paper, the authors gives the mean-field equations for this model, which they then proceed to solve numerically based on an iterative algorithm adapted from Turkington and Whitaker. To solve the mean-field equation in this setting, the domain needs to be finite, and suitable boundary conditions applied based on the known exact solution for the far-field stream function and potential vorticity.

The point vortex Monte Carlo method provides an alternate approach to solving the mean field equations. Using this approach, we can do away with any assumptions on the far-field stream function and potential vorticity.

The approach and results in this paper can be viewed from two different but related points of view. First, in view of the fact that a complete proof of the asymptotic exactness of the mean field equations in [1] is not yet available (although there should be no problem supplying one), we go behind the scene of these mean field equations and work with the ensemble of particles in the Heton model. The second point of view is to take the mean field equations in [1] as given and our approach then offers a very fast and efficient numerical method to solve these nonlinear elliptic PDEs.

This paper is organized as follows: in section two we collect all the equations and mention some of their consequences. Section three describes the Monte Carlo algorithm. Section four compares the Monte Carlo algorithm with the exact solution of the vorticity equations at inverse temperature $\beta = 0$. The numerical results gathered by the Monte Carlo simulations for positive and negative β are presented in sections five and six respectively.

2 Two layer quasi-geostrophic vorticity equations

DiBattista and Madja [1] presents a comprehensive discussion on the two species point vortex model of the two layer quasi-geostrophic vorticity equations. In this model, the stratified fluid which is permitted to evolve in the

unbounded plane, is partitioned into two thin slabs, each of constant depth, density and temperature. We shall not reproduce their discussions here, instead we collect only the necessary equations for our modeling purposes. The reader is referred to several relevant papers for the geophysical origins of this theory: [2], [4] , [5], [3], [7] , [6] , [8] , [9], [10].

The two layer quasi-geostrophic vorticity model give rise to the following conserved quantities:

$$
\begin{aligned}
Q_A &= \int_{R^2} q_A, && (1)\\
Q_B &= \int_{R^2} q_B, && (2)\\
H &= \sum_{j=A,B} -\frac{1}{2}\int_{R^2} \psi_j q_j, && (3)\\
\Gamma &= \sum_{j=A,B} \int_{R^2} q_j \left|\mathbf{x}^2\right|. && (4)
\end{aligned}
$$

$q_A(\mathbf{x})$ and $q_B(\mathbf{x})$ are the vortex density of the upper and lower layers respectively. In this paper, we shall only consider positive vorticity, $q_i(\mathbf{x}) > 0$ for all $\mathbf{x}$. ψ_A and ψ_B are the stream functions on the upper and lower layers respectively. They are coupled through the relations:

$$
\begin{aligned}
q_A &= \Delta\psi_A - (F\psi_A - F\psi_B) \quad \text{and}\\
q_B &= \Delta\psi_B + (F\psi_A - F\psi_B).
\end{aligned}
$$

where Δ denotes the horizontal Laplacian operator and F is related to the Rossby radius L_ρ by

$$F = \frac{1}{L_\rho^2}.$$

Conserved quantities (1) and (2) follows from the separately conserved circulation of each layer. The quantity H is the pseudo-energy of the vortex system. Γ is the angular momentum which is conserved as a consequence of the rotational invariance of the infinite plane.

The important role of angular momentum in the confinement of the baroclinic vortices to a bounded region, highlighted in [1], is based on a rigorous

mathematical result for the Heton Model in [10], which gives as sufficient condition for boundedness of baroclinic vortex dynamics, the nonzero sum of the total circulations of the two layers in the model.

2.1 Point vortex model

To allow numerical simulations of the two layer quasi-geostrophic model, we need to discretise the vortex field. We represent q_A and q_B with N discrete point vortices in each layer. That is, there are $2N$ numbers of point vortices. N of them belongs to the upper layer, each with vorticity $\omega_A = Q_A/N$; and the remaining N to the lower layer, each having vorticity $\omega_B = Q_B/N$. This representation automatically ensures that the total circulation of each species is separately conserved. Using point vortices to represent a continuous density distribution leads to a delta-function like vorticity profile. The probability of locating a point vortex in a certain finite area near $\mathbf{x}$ can be interpreted as the vortex density $q(\mathbf{x})$ in that area. And as $N \to \infty$, we expect this density to converge to the continuous vorticity densities q_A and q_B.

The discretised version of the pseudo-energy (3) would be:

$$\begin{aligned} H &= -\frac{\omega_A^2}{2}\sum_{i\neq j}\left[G_B\left(\mathbf{x}_i,\mathbf{x}_j\right)+G_T\left(\mathbf{x}_i,\mathbf{x}_j\right)\right] \\ &\quad -\frac{\omega_B^2}{2}\sum_{m\neq n}\left[G_B\left(\mathbf{x}_m,\mathbf{x}_n\right)+G_T\left(\mathbf{x}_m,\mathbf{x}_n\right)\right] \\ &\quad -\frac{\omega_A\omega_B}{2}\sum_{i\neq m}\left[G_B\left(\mathbf{x}_i,\mathbf{x}_m\right)-G_T\left(\mathbf{x}_i,\mathbf{x}_m\right)\right] \end{aligned} \tag{5}$$

and that for the angular momentum (4):

$$\Gamma = \omega_A\sum_i \mathbf{x}_i^2 + \omega_B\sum_m \mathbf{x}_m^2. \tag{6}$$

In the above, the subscript i and j denotes vortices of upper layer while m and n denotes the lower layer. G_B and G_T are the Green's functions for the barotropic, $(q_A+q_B)/2$ and baroclinic, $(q_A-q_B)/2$ vorticity field respectively. They are given by[1]:

$$
\begin{aligned}
G_B(\mathbf{x}_i, \mathbf{x}_j) &= \frac{1}{2\pi} \log |\mathbf{x}_i - \mathbf{x}_j| , \\
G_T(\mathbf{x}_i, \mathbf{x}_j) &= -\frac{1}{2\pi} K_0 \left(\sqrt{2F} \, |\mathbf{x}_i - \mathbf{x}_j| \right) .
\end{aligned}
$$

K_0 is the zeroth order modified modified Bessel function of the second kind.

2.2 Properties of H

In this section, we shall examine the actions of H in eqn (5) on a two vortex system.

For two vortices far apart, the K_0 component of their interaction vanishes and the Hamiltonian H tends to separate them even further. H then does not distinguish between the two layers. Hence for a vortex system where the number of vortices is small, and the distance between vortices is large, the system then effectively behaves like a single species system with total vorticity $N(\omega_A + \omega_B)$.

Next consider two vortices close to each other such that the effects of K_0 cannot be disregarded. Now vortex from the upper layer sees other vortices from the same layer differently as those from the lower layer. Hence we shall consider the inter-species interaction and the intra-species interaction separately.

In the **same species**, both the log and K_0 terms of the Hamiltonian again acts to push the vortices apart:

$$
H_{AA}(r_{ij}) = \frac{\omega_A^2}{4\pi} \left[-\log r_{ij} + K_0 \left(\sqrt{2F} r_{ij} \right) \right] .
$$

However for **different species**, the log term causes the vortices to repulse, while the K_0 term causes them to attract each other. Expanding the K_0 term as a Taylor series about the separation between the two vortices, $r_{im} = 0$, we get

$$
\begin{aligned}
H_{AB}(r_{im}) &= \frac{\omega_A \omega_B}{4\pi} \left[-\log r_{im} - K_0 \left(\sqrt{2F} r_{im} \right) \right] \\
&= \frac{\omega_A \omega_B}{4\pi} \left[\left(\gamma - \frac{1}{2} \log 2 + \frac{1}{2} \log F \right) \right. \\
&\quad \left. + \frac{r_{im}^2 F}{2} \left(\gamma - 1 - \frac{1}{2} \log 2 + \frac{1}{2} \log F + \frac{1}{2} \log r_{im} \right) + O\left(r_{im}^4 \right) \right] .
\end{aligned}
$$

Since $\log r_{im}$ is negative, we conclude that the two components acts together to cause a net Hamiltonian like $-r_{im}^2$. This produces a net repulsion between two vortices of different species.

So in all cases, the Hamiltonian would cause every vortex to move away from the other vortex. This can also be seen by observing that the gradient of $H(r)$ is always negative.

2.3 Equilibrium statistical mechanics

From the point of view of equilibrium statistical mechanics, the point vortices can take any accessible configuration, but each with a certain probability. The probability of a $2N$ vortex configuration $\vec{z_N}$ is given by:

$$P\left(\vec{z_N}\right) = \frac{\exp\left\{-\beta H\left(\vec{z_N}\right) - \mu\Gamma\left(\vec{z_N}\right)\right\}}{\int \exp\left\{-\beta H\left(\vec{z_N}\right) - \mu\Gamma\left(\vec{z_N}\right)\right\} d\vec{z_N}}. \tag{7}$$

β and μ are the Lagrange multipliers associated with the conservation of H and Γ respectively. When a vortex is located far from the origin, the quantity $\Gamma\left(\vec{z_N}\right)$ becomes large. From (7) we see that although the probability of a vortex being found far from the origin is non-zero (except when $\mu = \infty$), it is exponentially small.

Since each vortex lives in a two dimension space, the whole model has $4N$ dimensions. To explicitly calculate the probability of each configuration $\vec{z_N}$ we need to find the denominator of (7). This involves an integration over $4N$ dimensions. Although it is conceivable that one could attempt to calculate this quantity numerically by first restricting each two dimensional plane to a large enough domain. Then discretise this domain into a mesh of small finite areas, and finally add up all the contributions from all possible permutations of vortices in this discrete mesh. This direct calculation would require enormous computational power.

Instead, we proceed in a different direction. We use a Monte Carlo algorithm to generate a Markov chain of states. And from this finite collection of states, we deduce the equilibrium statistical properties of the model.

3 Monte Carlo algorithm

The implemented Monte Carlo algorithm is the standard Metropolis algorithm. The algorithm begins with $2N$ vortices, N of each type, placed ran-

domly on the disk of arbitrary radius. The formulation of the model in terms of point vortices ensures the conservation of total circulation in each layer. While not strictly necessary, we set the number of vortices of species A equal to the number of vortices of species B in all the simulations. The simulation proceeds as follows.

Step 1: From the initial distribution, $\vec{Z_N}$, one vortex is picked randomly from the $2N$ vortices.

Step 2: This vortex is then displaced in a random direction by a fraction of a preset maximum displacement. We call this new distribution $\vec{Z_N'}$. This small displacement would cause the vortex distribution to have a new augmented energy

$$E\left(\vec{z_N'}\right) = \beta H\left(\vec{z_N'}\right) + \mu\Gamma\left(\vec{z_N'}\right) \ .$$

Step 3: This new distribution will be accepted or rejected based on the following rule:

$$\begin{array}{rll} \text{if} & \exp\left(-\Delta E\right) > I & \text{, accept,} \\ & \text{otherwise} & \text{, reject.} \end{array}$$

ΔE is the difference of augmented energy between the new distribution and the old distribution. I is a uniformly distributed number between 0 and 1. If the new distribution is accepted, set $\vec{z_N} = \vec{z_N'}$, and repeat step 1. Otherwise discard $\vec{z_N'}$ and repeat step 1 with a new random vortex and displacement. N cycles of the loop constitute one sweep. The loop is exited after a large enough predetermined number of sweeps is reached.

The initial distribution is allowed to evolve for 100000 sweeps to relax, after which the simulation is sampled after every 50 subsequent sweeps.

At each sampled configuration, properties of the N vortex configuration like its energy, angular momentum and radial distribution was measured. The mean radial distribution for the whole run is then obtained by taking the average over all the sampled configurations.

These numerical simulations were carried out on a 2.2GHz Intel Xeon processor computer with 1 GB memory.

When doing physical experiments, the energy and angular momentum of the system is fixed (although it may be fluctuating with time). Then the Lagrange multipliers β and μ are measured using some measuring devices.

With this values, the physical quantities associated with each multiplier, energy and angular momentum is inferred. However in doing Monte Carlo simulations, we proceed the other way round. These multipliers are fixed, and the energy and momentum of the system is the quantity that is measured directly.

In all the simulations, we have set the Rossby radius to one.

4 Zero inverse temperature

We begin our discussions with the simplest case, $\beta = 0$. At zero inverse temperature, there is no Hamiltonian interaction between vortices. Essentially, each vortex in the system moves independently from the rest. With no interaction between vortices, there is no force that keeps them apart. The angular momentum however is still in effect, and it is easily seen that the lowest augmented energy state has $\Gamma = 0$ and $E = 0$. This is attained when all $2N$ vortices lies exactly on the origin.

In the Monte Carlo algorithm, the decision to accept or reject a proposed move depends only its resulting change in energy. And since at each move, only one vortex is displaced, the resulting change of energy is just

$$\omega \left(r^2_{i-new} - r^2_{i-old} \right) \ ,$$

where ω is the vorticity of the displaced vortex. It does not depend on the positions of any of the other vortices.

For zero β, any move that brings a vortex closer to the origin would always result in a lower augmented energy, and consequently the move would be accepted.

4.1 Barotropic flow

The Heton model is termed barotropic when the vorticity of both layers are equal, $\omega_A = \omega_B$. In fact at $\beta = 0$, the vortex model is solvable. The probability of finding a vortex of strength ω at r (distance measured from the origin) would be:

$$P(r) = \frac{\exp\left(-\mu\omega r^2\right)}{Z},$$

where μ is the Lagrange multiplier associated with the angular momentum. Z is a normalization factor

$$\begin{aligned} Z &= \int_{R^2} \exp\left(-\mu\omega r^2\right) \\ &= \frac{\pi}{\mu\omega}. \end{aligned}$$

Hence the vorticity profile of a single vortex is then

$$q = \frac{\omega}{\pi L^2} \exp\left(-\frac{r^2}{L^2}\right) \tag{8}$$

where we had introduced

$$L^2 = \frac{1}{\mu\omega}.$$

This is a Gaussian distribution with standard deviation L. The expected angular momentum of the single vortex would be:

$$\begin{aligned} \langle \Gamma(q) \rangle &= \int_{R^2} \omega r^2 P(r) \\ &= \frac{1}{\mu} \end{aligned} \tag{9}$$

The above eqn (9) can also be obtained directly from $\langle \Gamma(q) \rangle = -\partial \log Z / \partial \mu$. In doing the Monte Carlo simulations, we fix the Lagrange multiplier μ, and from there measure the energy of the system. However an alternative way of looking at it; from the usual method of Lagrange multiplier is that the angular momentum of the system is fixed at Γ. The Lagrange multiplier is then determined by substituting the solution (8) back into (6). Doing this we would again obtain the same results

$$\mu = \frac{1}{\Gamma}.$$

Having N identical vortices would result in a vorticity profile with the same spread, only N times stronger:

$$q^N = \frac{N\omega}{\pi L^2} \exp\left(-\frac{r^2}{L^2}\right). \tag{10}$$

The expected angular momentum of the system is N times greater than that of the single vortex

$$\left\langle \Gamma\left(q^N\right)\right\rangle = \frac{N}{\mu}. \tag{11}$$

We see from (11) that in the discrete case of N vortices, the angular momentum depends on the number of point vortices used to model the system. However for the angular momentum quantity to be meaningful, it should only depend on the physical property of total circulation $Q = N\omega$. Only Q appears in the continuous model, N and ω were artificially introduced during the discretization of the continuous vortex profile. The way to correct this would be to scale the Lagrange multipliers β and μ appropriately by a factor of N. But in this paper, we shall not be concerned with the scaling of the multipliers. For here, we do not make any comparisons with varying N and only a few cases of different N will be discussed.

4.2 Baroclinic flow

With two species of different vorticity, the flow is called baroclinic. However at $\beta = 0$, the analysis above follows with little change. The most probable vortex profile would two independent Gaussian:

$$\begin{aligned} q_A^N &= \frac{N\omega_A}{\pi L_A^2}\exp\left(-\frac{r^2}{L_A^2}\right), \\ q_B^N &= \frac{N\omega_B}{\pi L_B^2}\exp\left(-\frac{r^2}{L_B^2}\right) \end{aligned}$$

where

$$\begin{aligned} L_A^2 &= \frac{1}{\mu\omega_A}, \\ L_B^2 &= \frac{1}{\mu\omega_B}. \end{aligned}$$

Table (1) gives a comparison of the vorticity profile obtained by the Monte Carlo simulations using $N = 1$ with the exact results. 2×10^9 sweeps were used and a typical run takes about 1400 seconds.

μ	Height	Std dev	$\langle\Gamma\rangle$	$\frac{N\omega}{\pi L^2}$	L	$\frac{N\omega}{\mu}$
1	0.3201081	0.996964	0.9792	0.3183	1	1
2	0.638957	0.705566	0.4982	0.6366	0.7071	0.5
3	0.958247	0.576113	0.3327	0.9549	0.5774	0.3333
4	1.2749	0.499584	0.2497	1.273	0.5	0.25

Table 1: Comparison of Monte Carlo with exact values for $\beta = 0$ with $N = 1$. In the Monte Carlo simulation, we used $\omega_A = 1$. The first three columns gives the results on the Monte Carlo runs, while the last three are exact theoretical results. The total number of sweeps was 2×10^9.

Figure (1) shows the mean vorticity profile with $\mu = 2$. For this and all subsequent figures, we take radial symmetry of the profile to be given and plot only the radial variations. The kurtosis, β_2, of the profile was measured using:

$$\beta_2 = \frac{\mu_4}{\mu_2} ,$$

where μ_i is the i-th central moment. The discrete central moment is obtained from

$$\mu_i = \frac{\sum_j x_j r_j^i}{\sum_j x_j} ,$$

where firstly we discretise the profile into a finite number of bins, and then x_j is the height of the radial profile at the bin of distance r_j from the center. The sum for the central moment is taken over all the non zero radial bins.

In the figure, we see that the Monte Carlo results closely match the exact results.

Repeating this experiment with bigger N gives similarly accurate results. The profiles obtained were similar Gaussians, with amplitudes as predicted by (10). These results shall not be presented here.

Only when $\beta = 0$, can we make such comparisons. Explicit solutions for other values of β is not known. In fact for $\beta = 0$, what is taking place is equivalent to a random walk.

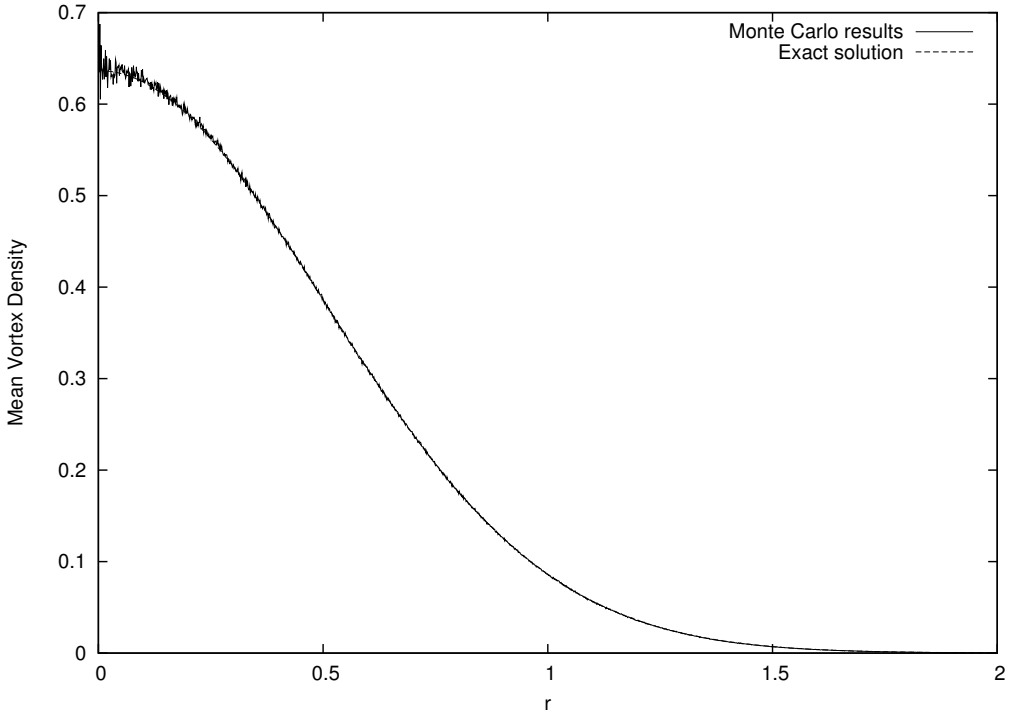

Figure 1: Comparison of the mean vortex density as obtained from the Monte Carlo simulations with the exact solution when $\omega_A = 1$, $\beta = 0$, $\mu = 2$ and $N = 1$. The two profiles coincide closely and are virtually indistinguishable. The Monte Carlo results were obtained from samples gathered after 2×10^9 sweeps. The Monte Carlo profile have a kurtosis of 3.0056, close to that of a true Gaussian.

5 Positive β

The next set of experiments deals with positive β. Figures (2)-(6) shows four simulations with $N = 60$, $\beta = 1$ and $\mu = 1$. ω_A is fixed at 1, while ω_B varies from 1 to 4. Each simulations involves 5 million sweeps took approximately 33000 seconds.

The vertical axis shows the vortex density of species B. The profile for species A have been scaled to match that of species B.

We see that the two profiles differ; on average they are not equally mixed. When $\omega_A \neq \omega_B$, species A (having a higher circulation) is more concentrated in the central region, while species B shows a more flat profile. As ω_B increases both vortex density profiles gradually flattens and its kurtosis approaches 1.8, the value for a uniform distribution.

Furthermore, when ω_A and ω_B are fixed as β increases, the vortices of both species tends to a uniform distribution of the same radial support. Figure (7) plots the distance of the furthest vortex from the origin in the final vortex configuration against β for large values of β.

6 Negative β

For negative β, the highest attainable energy configuration is for all the vortices to clump together, forming a singularity at the origin. This is also true for the case when $\beta = 0$.

However when

$$\beta > -\frac{8\pi}{N \max\{\omega_A, \omega_B\}},$$

the partition function $Z(N)$ still remains finite, and hence the probability measure (7) is still valid. Therefore we would still have a finite probability of a vortex configuration with non-zero support.

Recall that the inverse temperature is proportional to the derivative of entropy vs. energy, and the more negative T is, the less hot it is. In statistical mechanics at negative temperatures, it is usually the maxima of the free energy of the system, $F = E - TS$ that determines the most probable state; in other words, the most probable state usually corresponds to a state of maximum entropy, whether the temperature is positive or negative. But under certain conditions, this most probable state is close to maxima of the

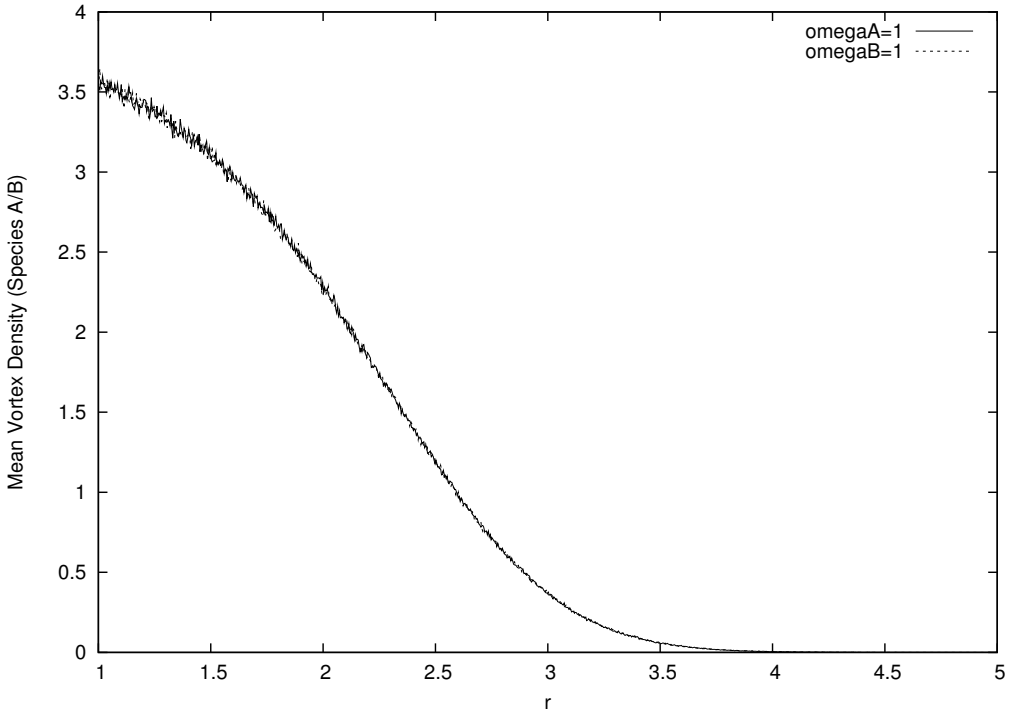

Figure 2: Mean vortex density from 60 vortex of species A and 60 of species B. Both species have equal vorticity,$\omega_A = \omega_B = 1$. The values $\beta = 1$, $\mu = 1$. Since both species have the same vorticity, their mean density profile is also the same. They are flatter than the Gaussian with a kurtosis of 2.2324 and 2.2396 for species A and B respectively.

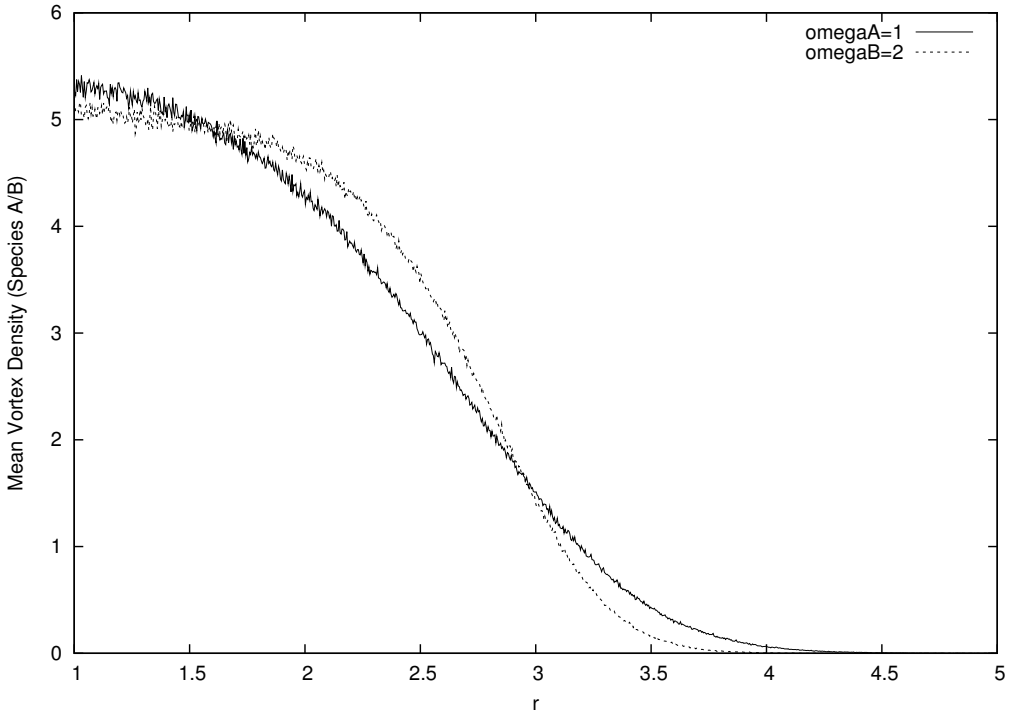

Figure 3: Vorticity profile for $\omega_A = 1$ and $\omega_B = 2$. $\beta = 1$ and $\mu = 1$. Comparing with figure 2, both profiles are significantly flattened despite the vortex strength of species A being unchanged. Kurtosis of species $A = 2.1548$, and species $B = 1.9798$.

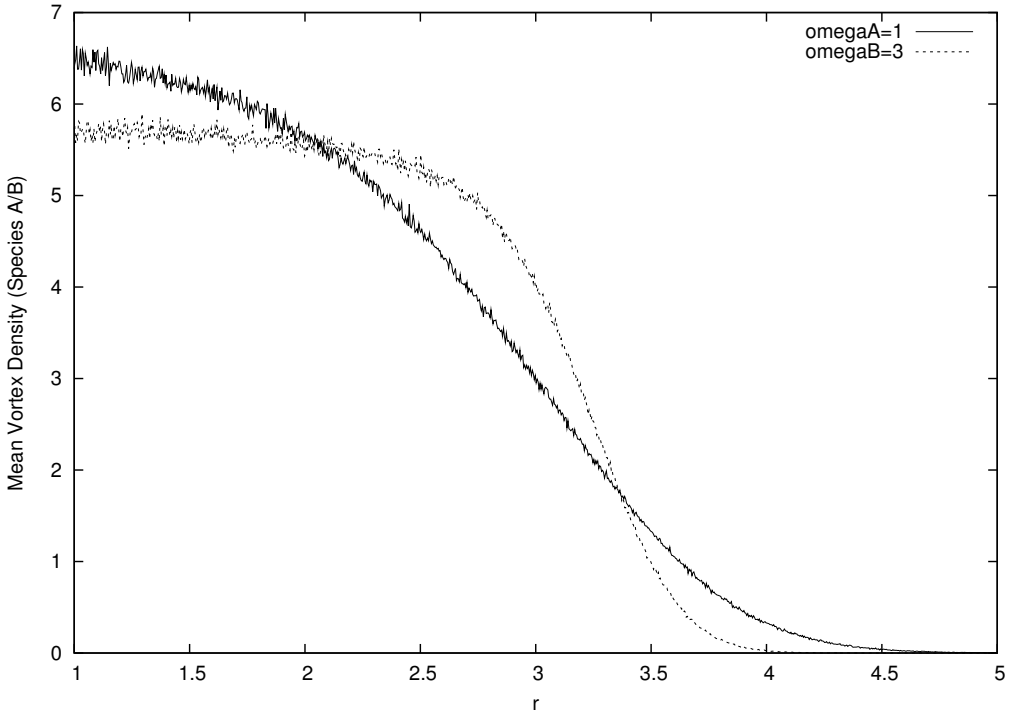

Figure 4: Vorticity profile for $\omega_A = 1$ and $\omega_B = 3$. $\beta = 1$ and $\mu = 1$. Kurtosis of species $A = 2.1221$, and species $B = 1.8920$.

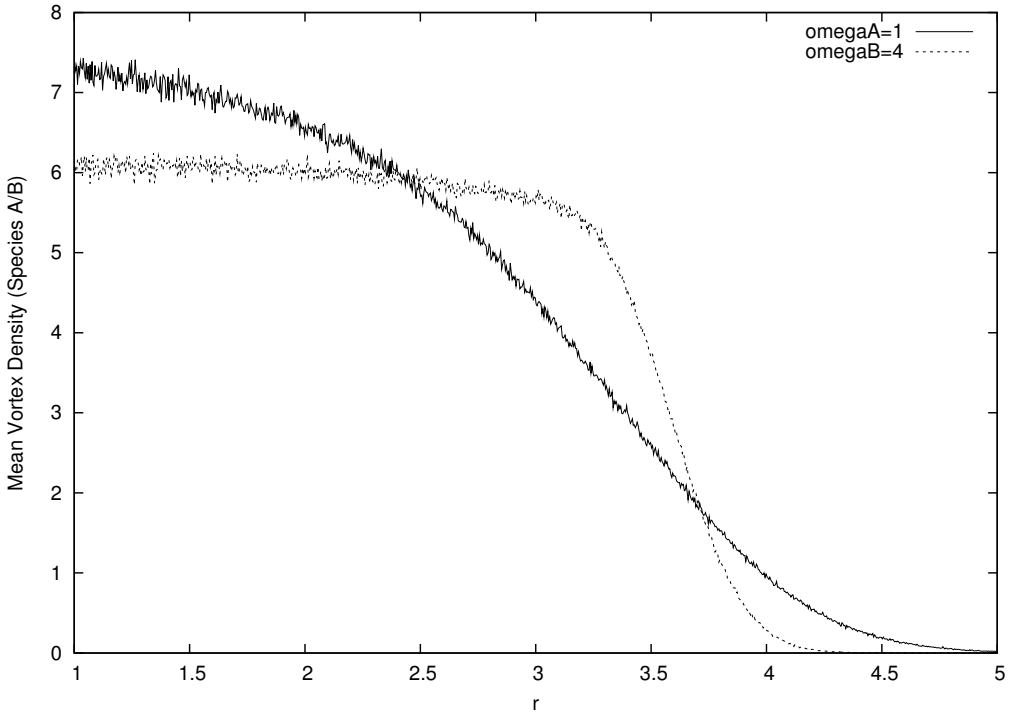

Figure 5: Vorticity profile for $\omega_A = 1$ and $\omega_B = 4$. $\beta = 1$ and $\mu = 1$. Kurtosis of species $A = 2.0950$, and $speciesB = 1.8560$.

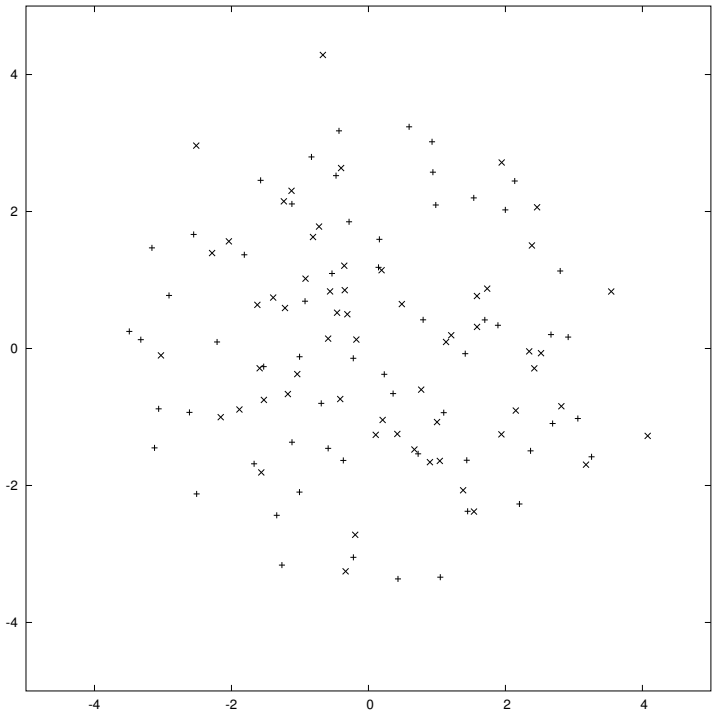

Figure 6: The vortex distribution at the final sweep with $N = 60$, $\beta = 1$, $\mu = 1$, $\omega_A = 1$ ('+') and $\omega_B = 4$ ('x').

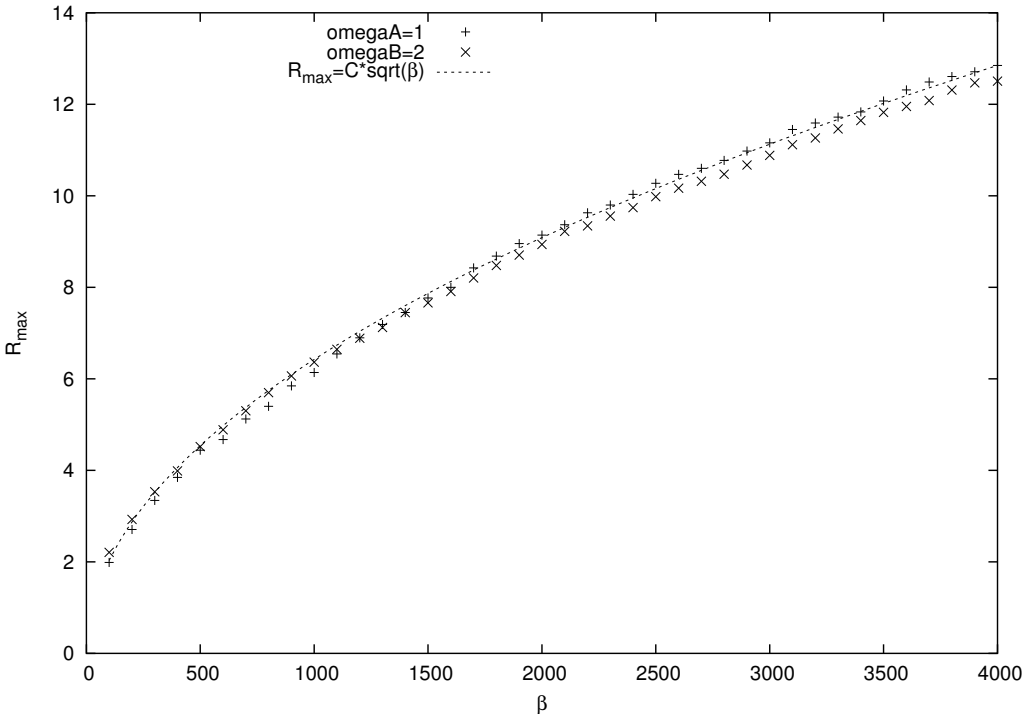

Figure 7: Graph of R_{max} vs β showing the relationship $R_{max}^2 \sim \beta$. At these values of β, the vorticity profile of both layers are nearly uniform (flat top).

energy E. We have seen that for low positive temperatures, this approximation principle holds in the Onsager Point Vortex gas, and it is expected to be valid also for the Heton Vortex Gas at low positive temperatures.

This situation arises near the singularity at extremal negative temperature T_0: the distribution of vortices all lumped together near the singularity has very low entropy S, but extremely high energy; any other macro-state will have larger entropy but smaller energy, leading to a smaller free energy, because the extremal temperature T_0 has the smallest allowed numerical value when it is negative. Moreover, its temperature T_0 being negative and of the smallest allowed numerical value means that the derivative of entropy with respect to the energy is negative, and a decrease of energy will lead to the largest corresponding increase of entropy for a neighboring macro-state at a slightly more negative value for T. Thus, for negative temperatures which have large numerical values, the energy of the most probable state must decrease as the entropy increases, and the approximation principle is not valid.

The simulation results in the following subsections support the above scenario of a continuous change from the energy dominated state at the extremal negative temperature to a balanced combination of higher entropy and lower energy states at negative temperatures with large numerical values.

We do not have a finite temperature cutoff for positive temperatures, and the above approximation principle holds for different reasons than here. At very low positive temperatures, minimizers of the free energy are identical to minimizers of internal energy but they are also entropy maximizers since these macro-states are essentially radial uniform states. As the positive temperature increases, the minimizers of the free energy shifts continuously towards the Gaussian profiles which have lower entropy and higher energy. The numerical results on the Heton Gas at positive temperatures in sections 4 and 5 support this overall picture.

6.1 Barotropic flow

Figures (8) and (9) shows the mean vortex density and the final distribution of a barotropic Monte Carlo simulation with $N = 80$, $\mu = 1$ and $\beta = -0.1$. In this run the vortex strengths $\omega_A = \omega_B = 1$. As expected both species has the same radial profile. A Gaussian plot for $\beta = 0$ is included for comparison. When β is negative, the vortex density profile is more concentrated in the central region compared to the Gaussian. This is also reflected in the kurtosis

of the density profile which is greater than three.

The simulation was carried out for two million sweeps and took about 12000 seconds.

6.2 Baroclinic flow

Figures (10) and (11) shows the mean vortex density and the final distribution of a baroclinic Monte Carlo simulation with the same parameters as before: $N = 80$, $\mu = 1$ and $\beta = -0.1$. But in this run we have $\omega_A = 1$ and $\omega_B = 2$. The vortices of both species becomes more concentrated near the origin as ω_B increases.

In the regime

$$\beta < -\frac{8\pi}{N \max\{\omega_A, \omega_B\}},$$

the partition function is not well defined. However we can still do Monte Carlo runs with such large negative β; after all its just a matter of changing a variable for the computer simulation. And knowing that the system will be ill behaved, the result should not be taken too seriously. If we insist on doing so, we get a vortex configuration with all the vortices moving closer and closer together until the simulation reaches the total number of sweeps or until the simulation breaks down due to a large negative energy that is beyond the computer's capability to handle.

7 Conclusion

We conclude with a few specific physical points which are worth following up in future works. They are:

(A) As the vortex strength of species B gets progressively larger with respect to species A (cf. Figures 2 - 6), the equilibrium distributions of both species become closer to a flat-top radial distribution.

(B) For any fixed ratio of vortex strengths that is not too extreme, the simultaneous appearance of both canonical types of vorticity distributions at a single positive temperature is remarkable. By canonical types we refer to the two main types of equilibrium vorticity distributions in the Onsager vortex gas on an unbounded plane, namely, the Gaussian-like radial distribution for relatively low values of β and the nearly flat-top radial distribution at higher

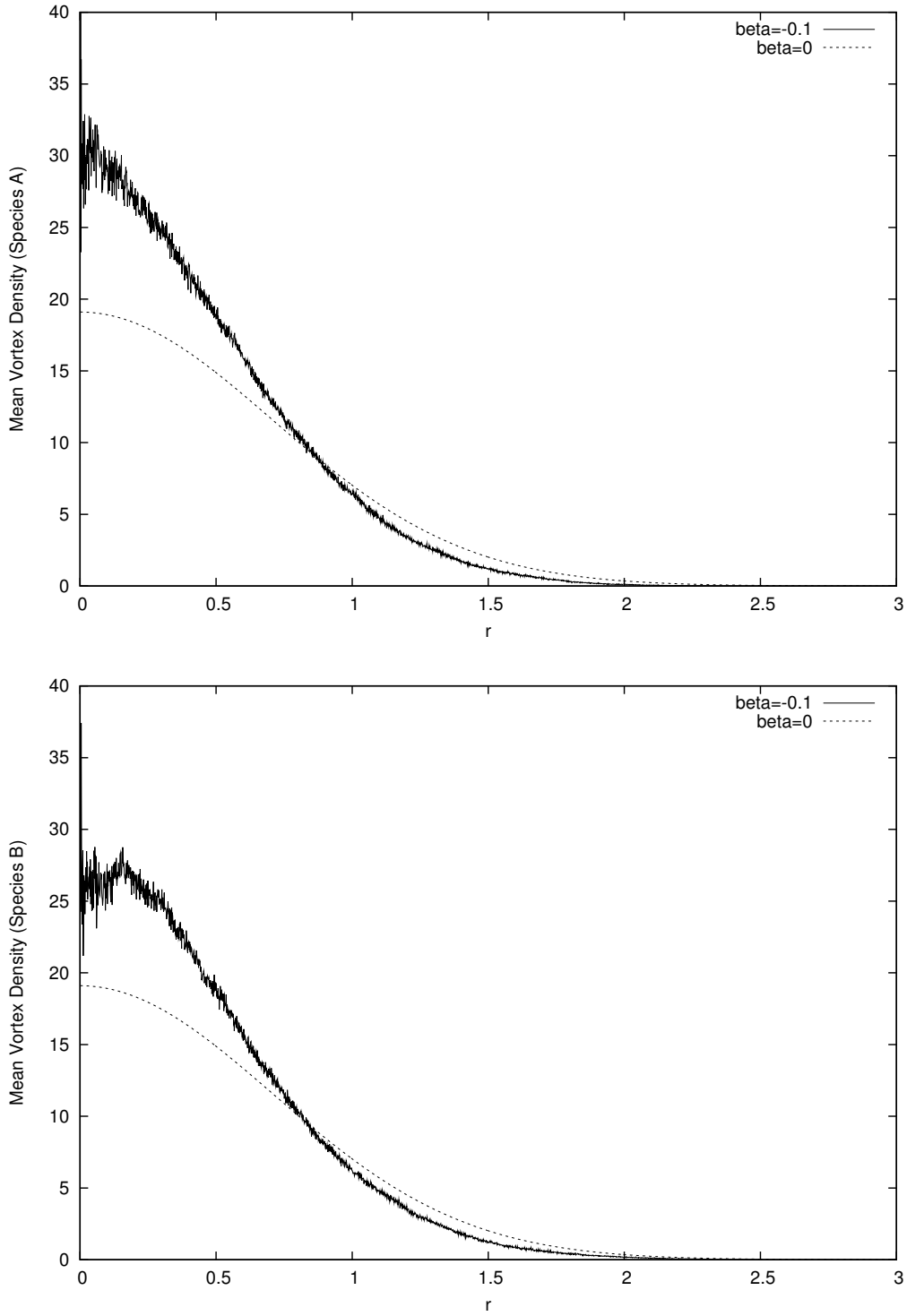

Figure 8: Mean vortex density of 80 vortices per species, with a negative $\beta = -0.1$ and $\mu = 1$. Both species have the same vorticity, $\omega_A = \omega_B = 1$. The dotted lines gives the Gaussian solution when $\beta = 0$. Kurtosis of $A = 3.1488$ and kurtosis of $B = 3.2352$.

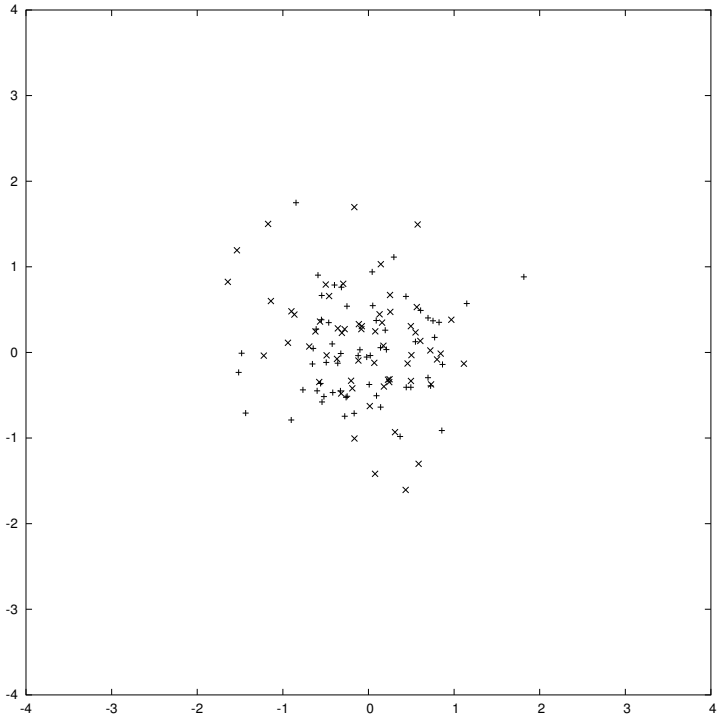

Figure 9: The distribution of 160 vortices with $\mu = 1$ and a negative $\beta = -0.1$ after 2 million sweeps. Both species have the same vorticity, $\omega_A = \omega_B = 1$.

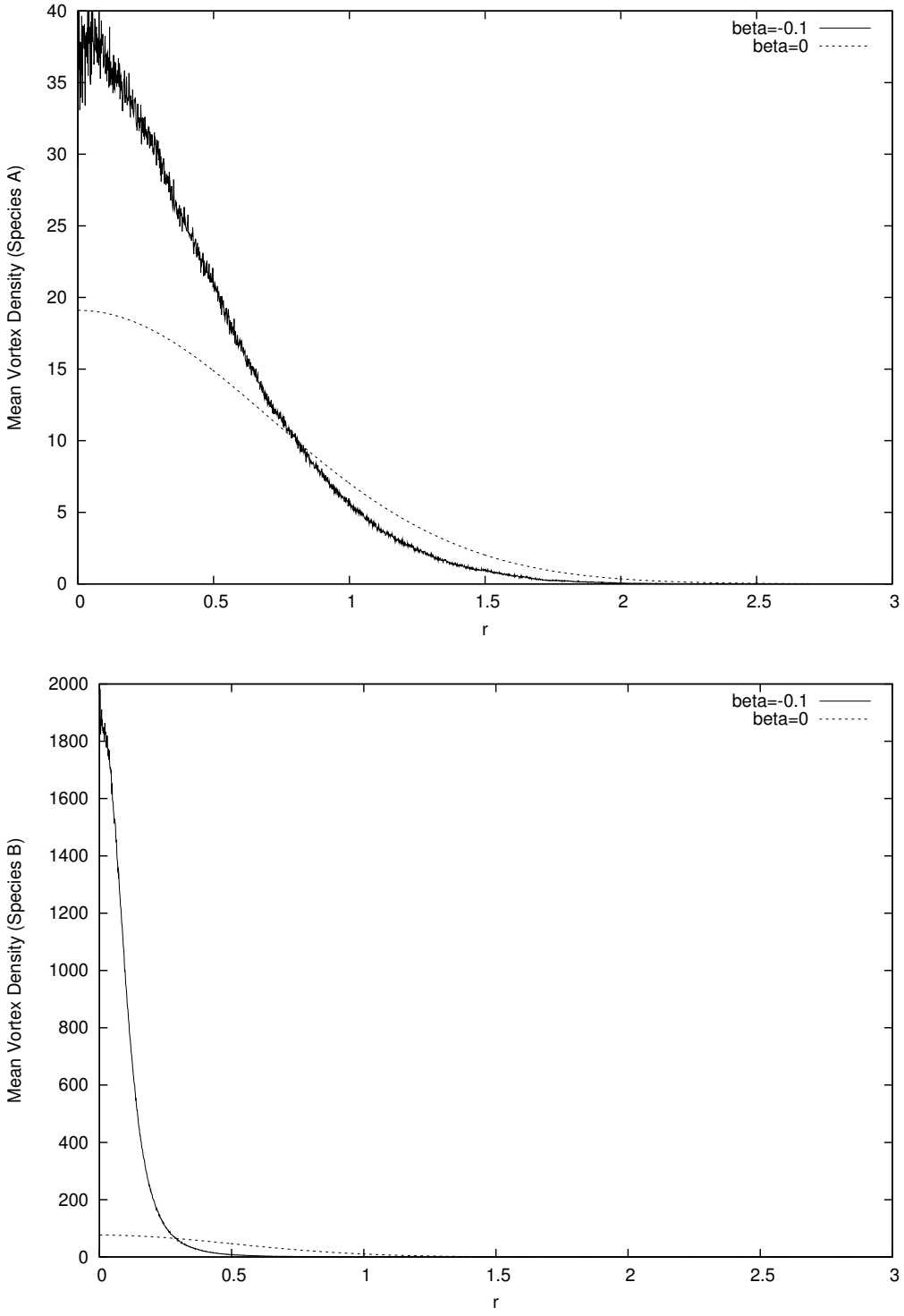

Figure 10: Mean vortex density of 60 vortices per species with a negative $\beta = -0.1$ and $\mu = 1$. $\omega_A = 1$ and $\omega_B = 2$. The dotted lines gives the Gaussian solution when $\beta = 0$. Kurtosis of $A = 3.3507$ and kurtosis of $B = 11.455$. A two fold difference in ω causes a large 50 times difference in the vortex concentration at the center.

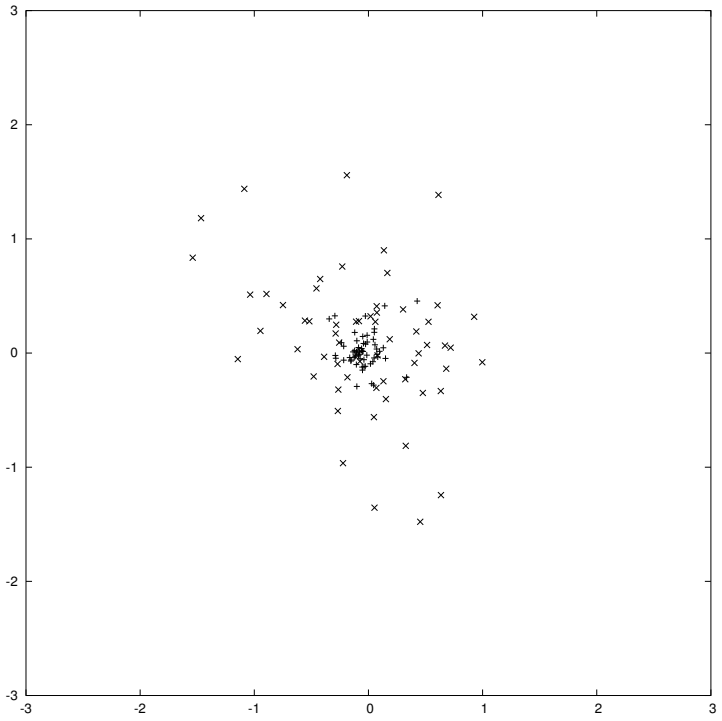

Figure 11: The distribution of 120 vortices with $\mu = 1$ and a negative $\beta = -0.1$ after 2 million sweeps. Species A ('x') has vorticity $\omega_A = 1$ while for species B ('+'), $\omega_B = 2$. The '+' vortices are more highly concentrated in the central region.

values of β. In the Onsager vortex gas as well as in its exact mean field theory, the Gaussian type was found analytically, but the flat-top type was discovered in numerical solutions [11] of the mean field equations. We refer the reader to recent papers [11] and [12] which discuss these canonical types in detail. In particular, [12] gives a rigorous energy variational formulation for the flat-top radial solutions within a low temperature approximation to the mean field equations for the Onsager vortex gas. This approximation is based on the idea that at low positive temperatures, the Helmholtz Free energy, $F = E - TS$, is dominated by the augmented internal energy E.

(C) For any fixed vortex strength ratio, the radial profiles of both species tend towards the flat-top uniform one as the positive inverse temperature increases.

(D) The power law of the radii of vorticity supports suggests that they are proportional to the square root of the product of the respective circulations with the ratio of inverse temperature to chemical potential

$$R \sim \sqrt{\frac{\beta\omega}{\mu}} \, .$$

As a direct result, this extended power law for the radii allows us to simulate the Heton statistics in any disk, at all values of the energy and total circulations, provided we are free to choose the chemical potential.

(E) The rigorous proof of such a power law (at least for low positive temperatures) can be constructed by minimizing an augmented energy functional, along the same lines as the proof in the Onsager Vortex Gas Problem. Similar to that proof, this will likely require a technical lemma on the existence of radially symmetric and compactly supported minimizers of the augmented energy functional. One should be able to prove such a lemma using techniques from the Direct Method of the Calculus of Variations.

(F) This power law for the radial extent of the cold temperature and potential vorticity anomalies confirms that in a preconditioned barotropic gyre with sufficiently strong cyclonic signature, the baroclinic cooling is localized in an unbounded open ocean. DiBattista - Majda discovered a length scale L_A for the radial extent which is directly related to the angular momentum in the barotropic component, and to the $\beta = 0$ exact solution. Our power law with exponent $\frac{1}{2}$ in the quantity $\frac{\beta}{\mu}$ extends the relationship they found between L_A and angular momentum, to the $\beta > 0$ region. Through the power law's dependence on total circulations, inverse temperature beta and

chemical potential μ, we are able to predict the radial extent of the equilibrium cold temperature and potential vorticity anomalies as a function of the mean kinetic energy and mean baroclinic angular momentum in the localized open ocean convection site. These quantities can be related back to the meteorological conditions that preconditioned the ocean site, such as the wind stress that caused the cyclonic gyre, and the cold air reservoir for potential vorticity anomaly. In short, the doubly - canonical Gibbs ensemble used in the DiBattista - Majda model is optimal for the modeling of the most probable localized response of a stratified rotating flow interacting with a heat bath and an angular momentum reservoir simultaneously.

As discussed earlier, the Metropolis algorithm we used simulates this interaction between the flow and the heat and angular momentum baths through prescribed values of the temperature and chemical potential. The qualitative agreement between our results, namely the power law, and several numerical simulations (and experiments) showing that with a strong enough barotropic rim current, baroclinic instabilities can be suppressed in the dynamics of a rotating stratified system, motivates further work on the variational formulation and rigorous derivation of this numerical power law.

Acknowledgment

The work of Professor Chjan C. Lim was partially supported by ARO grant # W911NF-05-1-0001 and DOE grant # DE-FG02-04ER25616.

References

[1] Mark T. DiBattista, Andrew J. Majda, *"Equilibrium Statistical Predictions for Baroclinic vortices: The Role of Angular Momentum"*, Theor. Comp. Fluid Dyn. 14, 293-322, 2001.

[2] V.M. Gryanik, *"Dynamics of Localized Vortex Perturbations — "Vortex Charges" in a Baroclinic Fluid",* Isvestiya, Atmospheric and Oceanic Physics, Vol. 19(5), 347-352, (1983).

[3] I.M. Held, R.T. Pierrehumbert, S.T. Garner and K.L. Swanson, *"Surface quasi-geostrophic dynamics",* J. Fluid Mech. 282, 1-20, (1995).

[4] N.G. Hogg and H.M. Stommel, *"The Heton: an elementary interaction between discrete baroclinic vortices, and its implication concerning eddy heat flow",* Proc. Roy. Soc. Lond. A397, 1-20, (1985).

[5] N.G. Hogg and H.M. Stommel, *"Hetonic explosions: The breakup and spread of warm pools as explained by baroclinic point vortices",* J. Atmos. Sci., 42, 1465-1476, (1985).

[6] S. Legg and J. Marshall, *"A Heton model of the spreading phase of Open Ocean Deep Convection"*, J. Phys. Oceanography 23(6), 1040-1056, (1993).

[7] S. Legg, H. Jones, and M. Visbeck, *"A heton perspective of baroclinic eddy transfer in localized ocean deep convection",* J. Phys. Oceanogr. 26, 2251-2266 (1996).

[8] S. Legg and J. Marshall, *"The influence of the ambient flow on the spreading of convective water masses",* J. Mar. Res. 56, 107-139 (1998).

[9] J. Marshall and F. Schott, *"Open-ocean convection: Observations, theory and models",* Rev. Geophysics 37, 1-64 (1999).

[10] C.C. Lim and A.J. Majda, *"Point Vortex Dynamics For Coupled Surface/Interior QG And Propagating Heton Clusters In Models For Ocean Convection"*, Geophys. Astrophys. Fluid Dyn. Vol 94, Issues 3-4, 177-220, August, 2001.

[11] S.M. Assad and C.C. Lim, *"Statistical equilibrium of the vortex gas on the unbounded 2D plane"*, DCDS-B vol. 5(1), 2005.

[12] C.C. Lim and S.M. Assad, *"Self-containment radius for low temperature single-signed vortex gas and electron plasma",* preprint, 2004.